Brain, Behavior, and Immunity 49 (2015) 280–292

Contents lists available at ScienceDirect

Brain, Behavior, and Immunity

journal homepage: www.elsevier.com/locate/ybrbi

The choroid plexus transcriptome reveals changes in type I and II interferon responses in a mouse model of Alzheimer's disease

Sandro Dá Mesquita [a,b], Ana C. Ferreira [a,b], Fuying Gao [c], Giovanni Coppola [c], Daniel H. Geschwind [c], João C. Sousa [a,b], Margarida Correia-Neves [a,b], Nuno Sousa [a,b], Joana A. Palha [a,b], Fernanda Marques [a,b,*]

[a] Life and Health Sciences Research Institute (ICVS), School of Health Sciences, University of Minho, Campus Gualtar, 4710-057 Braga, Portugal
[b] ICVS/3B's – PT Government Associate Laboratory, Braga/Guimaraes, Portugal
[c] Program in Neurogenetics, Department of Neurology, David Geffen School of Medicine – University of California, Los Angeles, CA, USA

ARTICLE INFO

Article history:
Received 19 March 2015
Received in revised form 29 May 2015
Accepted 10 June 2015
Available online 16 June 2015

Keywords:
Alzheimer's disease
Aging
Memory
Choroid plexus
Transcriptome
Neuroinflammation
Interferons
Cerebrospinal fluid
Hippocampus
Glial cells

ABSTRACT

Alzheimer's disease (AD) is a neurodegenerative disorder characterized by a marked decline in cognition and memory function. Increasing evidence highlights the essential role of neuroinflammatory and immune-related molecules, including those produced at the brain barriers, on brain immune surveillance, cellular dysfunction and amyloid beta (Aβ) pathology in AD. Therefore, understanding the response at the brain barriers may unravel novel pathways of relevance for the pathophysiology of AD. Herein, we focused on the study of the choroid plexus (CP), which constitutes the blood–cerebrospinal fluid barrier, in aging and in AD. Specifically, we used the PDGFB-APPSwInd (J20) transgenic mouse model of AD, which presents early memory decline and progressive Aβ accumulation, and littermate age-matched wild-type (WT) mice, to characterize the CP transcriptome at 3, 5–6 and 11–12 months of age. The most striking observation was that the CP of J20 mice displayed an overall overexpression of type I interferon (IFN) response genes at all ages. Moreover, J20 mice presented a high expression of type II IFN genes in the CP at 3 months, which became lower than WT at 5–6 and 11–12 months. Importantly, along with a marked memory impairment and increased glial activation, J20 mice also presented a similar overexpression of type I IFN genes in the dorsal hippocampus at 3 months. Altogether, these findings provide new insights on a possible interplay between type I and II IFN responses in AD and point to IFNs as targets for modulation in cognitive decline.

1. Introduction

Alzheimer's disease (AD) is the most prevalent form of dementia and is predicted to affect eighty million people worldwide by 2040 (Ballard et al., 2011; Querfurth and LaFerla, 2010). The major constraint of AD patients is the severe loss of cognitive abilities (Ballard et al., 2011). Moreover, this neurodegenerative disease is characterized by two main brain pathological hallmarks: the extracellular deposition of amyloid beta (Aβ) peptides, in the form of senile plaques, and the formation of intracellular neurofibrillary tangles, as a result of increased aggregation of hyperphosphorylated Tau protein (Gotz et al., 2001; Hardy and Selkoe, 2002; Lewis et al., 2001; Scheuner et al., 1996). The amyloidogenic hypothesis of AD considers that amyloid pathology may result from increased Aβ production, through the amyloidogenic processing of the amyloid precursor protein (APP), and/or decreased excretion of Aβ out of the brain (Hardy and Selkoe, 2002; Roberson and Mucke, 2006). In fact, oligomerization of Aβ peptides in the brain has been described as an early pathogenic event that is responsible for behavior alterations (Mucke et al., 2000; Palop and Mucke, 2010). However, regardless of the attention given to increased Aβ formation and toxicity in the brain, neuroinflammation is also recognized as an early and essential mediator of brain pathology and behavior alteration in AD (Lucin and Wyss-Coray, 2009; Wyss-Coray, 2006). In this context, two relevant emerging concepts should be considered: (I) the age-associated changes in the blood composition and (II) the levels/ratio of type I and II interferon (IFN) cytokines. Regarding the first concept, recent observations showed the involvement of the systemic milieu in memory formation and the role of specific inflammatory molecules in age-related decreased synaptic plasticity and memory function (Baruch et al., 2013; Villeda et al., 2011). Regarding the second concept, an enhanced type I IFN signaling at the brain barriers, and

* Corresponding author at: Life and Health Sciences Research Institute (ICVS), School of Health Sciences, University of Minho, Campus Gualtar, 4710-057 Braga, Portugal.
E-mail address: fmarques@ecsaude.uminho.pt (F. Marques).

http://dx.doi.org/10.1016/j.bbi.2015.06.008
0889-1591/

decreased type II IFN response, have recently been implicated in cognitive decline in aged mice (Baruch et al., 2014).

Of relevance, the brain barriers, namely the blood–brain barrier, composed by the endothelial cells of the blood capillaries, and the blood–cerebrospinal (CSF) barrier, formed by the choroid plexus (CP) epithelial cells, seems to influence both the excretion of Aβ peptides out of the brain (Carro et al., 2002, 2005; Zlokovic, 2008) and the inflammatory response (Marques et al., 2009, 2013; Zlokovic, 2008). Particularly, besides its role in the formation and secretion of the CSF, recent studies clearly indicate that the CP is able to modulate the cognitive function, through changes in the neuroinflammatory response and in brain immune surveillance (Baruch et al., 2013, 2014; Baruch and Schwartz, 2013). Interestingly, the role of the CP in the neuroinflammatory response in AD, as well as its connection with impaired memory and cognition, is still poorly understood and is addressed in the present study. Specifically, we took advantage of a mouse model of AD that presents early cognitive deficits and brain amyloid pathology, the PDGFB-APPSwInd (J20) (Mucke et al., 2000), and respective wild-type (WT) age-matched littermates, to study changes in the CP transcriptome and in the composition of the CSF. Furthermore, we analyzed the extension of the changes observed at the level of the CP, by assessing the neuroinflammatory response at the dorsal hippocampus (dHPC), a brain region that is seriously affected in AD (Palop et al., 2007; Villeda et al., 2011). Altogether, the results suggest that alterations in IFN signaling may contribute to neuroinflammation, amyloid pathology and cognitive impairment in aging and in AD.

2. Materials and methods

2.1. Ethics statement

Animal handling and experimental procedures were conducted in accordance with the Portuguese national authority for animal experimentation, Direção Geral de Veterinária (ID: DGV9457). Animals were kept in accordance with the guidelines for the care and handling of laboratory animals in the Directive 2010/63/EU of the European Parliament and the Council. The animals were housed and maintained in a controlled environment at 22–24 °C and 55% humidity, on 12 h light/dark cycles and fed with regular rodent's chow and tap water *ad libitum*.

2.2. Animal model and experimental groups

Male hemizygous B6.Cg-Tg(PDGFB-APPSwInd)20Lms/2J/Mmjax (J20) mice, in a C57BL/6J background, first developed by Professor Lennart Mucke, of The J. David Gladstone Institutes (San Francisco, CA, USA), were purchased from The Jackson Laboratory (Bar Harbor, Maine, USA). The J20 mice express a mutant form of the human APP bearing both the Swedish (K670N/M671L) and the Indiana (V717F) mutations (APPSwInd). Expression of the transgenic insert is directed by the human platelet-derived growth factor beta polypeptide (PDGFB) promoter (Mucke et al., 2000). Hemizygous mice present the highest expression of the transgene product in neurons of the neocortex and HPC. At 5–7 months of age diffuse Aβ peptides deposition is detected in the dentate gyrus (DG) and neocortex. Amyloid deposition is progressive with all transgenic mice exhibiting plaques by the age of 8–10 months (Mucke et al., 2000; Palop et al., 2007). Both hemizygous transgenic J20 mice and age-matched non-carrier WT littermates (all males) were used. Male mice were divided, according to age, into three groups: 3 months, 5–6 months and 11–12 months. These ages were chosen in order to assess the changes in behavior, at the blood–CSF barrier and in the brain parenchyma, at different stages of Aβ pathology, particularly before and after Aβ plaque formation. The value of achieved power ($1-\beta$) of the sample was calculated using the IBM SPSS Statistics for Windows (Version 23.0. Armonk, NY: IBM Corp, USA), on the basis of the sample size ($N = 80$) and effect size (partial eta squared = 0.044) associated with the Morris water maze (MWM) test, which was analyzed by a parametric repeated measures two-way ANOVA ($\alpha = 0.05$). Taking that the Mauchly's Test revealed a violation of sphericity for the analyzed groups, the Huynh–Feldt correction was applied and a final value of $1-\beta = 0.841$ was obtained, which is considered to be statistically powerful (Mazen et al., 1985).

2.3. MWM paradigm

Memory was evaluated during the light phase of the diurnal cycle using the MWM paradigm. The MWM was performed in a white circular pool (170 cm in diameter and 50 cm in height), filled with tap water (23 ± 1 °C; 30 cm of depth) and placed in a poorly lit room. The water tank was divided into four imaginary quadrants (north, east, south, and west), each corresponding to a fixed extrinsic clue visible to the mouse. A transparent escape platform (14 cm in diameter and 30 cm high), invisible to the mouse, was placed in the center of one of the quadrants and was maintained in that same position during the five days of the acquisition. For spatial reference-memory acquisition, a HPC-dependent task, the mice were placed randomly in one of the quadrants in each trial, and allowed to search for the hidden platform. During the five days of the acquisition phase, each mouse performed four trials per day. Each trial was concluded when the platform was reached within the time-limit of 120 s. If failing to reach the platform within this time-period, the mouse was guided to the platform and allowed to stay in it for 30 s. The four random consecutive trials of each day were video-captured with a video-tracking system (Viewpoint, Champagne au Mont d'or, France) and the mean values of the time (latency to platform) and speed to reach the platform were calculated. To analyze the MWM performance, mice were divided into groups according to their age and genotype. After two independent experiments with identical results, the final number of mice per group was the following: at 3 months, N (WT) = 16 and N (J20) = 8; at 5–6 months, N (WT) = 8 and N (J20) = 10; at 11–12 months, N (WT) = 23 and N (J20) = 15.

2.4. Tissue sample collection and storage

During the light phase of the diurnal cycle, specifically in the morning, mice were anesthetized with an intraperitoneal injection of a mixture of ketamine hydrochloride (150 mg/kg, Imalgene® 1000) and medetomidine hydrochloride (0.3 mg/kg, Dorben®). Under deep anesthesia, CSF samples were collected from the cisterna magna and checked for blood contamination using a haemocytometer. Samples were stored at −80 °C until further use. After this, mice were transcardially perfused with 0.9% saline and the brains were removed from the skull. For gene expression analysis by microarray and qRT-PCR, the CP samples from each brain ventricle of the same mouse were rapidly removed under a conventional light stereomicroscope (SZX7, Olympus, Hamburg, Germany), pooled, snap-frozen and stored at −80 °C. Specific brain areas, namely the dHPC, were obtained by macrodissection, snap-frozen and stored at −80 °C, for RNA extraction and gene expression analysis. Whole brains were fixed in 4% paraformaldehyde (PFA, Panreac Química S.L.U., Barcelona, Spain) for 48 h and kept in paraffin blocks until further sectioning. Alternatively, brains were immediately embedded in Richard-Allan Scientific™ Neg-50™ Frozen Section Medium (ThermoFisher Scientific, Waltham, MA, USA), snap-frozen and kept frozen at −20 °C until further sectioning.

2.5. Microarray and Ingenuity® Pathway Analysis

Total RNA was extracted from CP tissue using the RNeasy® Plus Micro Kit (Qiagen, Hamburg, Germany), following the manufacturer's instructions. After quality assessment using the Agilent Bioanalyzer (Agilent Technologies, CA, USA), 500 ng of total RNA were used for T7-based mRNA amplification using the manufactured kit TargetAmp™ 2 – Round Biotin aRNA Amplification Kit 3.0 (Epicentre, Illumina, Wisconsin, USA), according to the manufacturer's instructions. The quality of amplified RNA was assessed using an Agilent Bioanalyzer. Amplified RNA was labeled and hybridized to Illumina Mouse Ref 8 v2.0 gene expression BeadChips, querying the expression of approximately 25,600 RefSeq-curated gene targets, for microarray analysis by the Southern California Genotyping Consortium (SCGC) core using the Illumina BeadStation platform. Statistical microarray analysis and gene expression analysis were performed at the Informatics Center for Neurogenetics and Neurogenomics (ICNN) core at UCLA using R (www.r-project.org) and Bioconductor (www.bioconductor.org) packages as described before (Coppola, 2011; Coppola et al., 2008). The raw data was deposited in the GEO database, accession number *GEO: GSE66598*. Gene pathway and functional analysis was performed using the Ingenuity Pathway Analysis 6.0 (IPA; Ingenuity® Systems, www.ingenuity.com). The CP transcriptome of WT mice at 3 ($N = 3$), 5–6 ($N = 4$) and 11–12 ($N = 6$) months, and of J20 mice at 3 ($N = 4$), 5–6 ($N = 4$) and 11–12 ($N = 3$) months, was analyzed and compared. The individual data sets consisted on: (I) the comparison between the CP transcriptome of J20 mice and the CP transcriptome of WT mice, at different ages; (II) the comparison between the CP transcriptome of 11–12 months-old mice and that of 3 months-old mice, for each genotype independently. The data sets containing the accession numbers, the log ratio and the *p*-value for each gene, whose expression was significantly changed (p-value < 0.05), were uploaded into the IPA database. Using IPA and its applications, each gene identifier was mapped and the genes were used to build networks associated with a specific canonical pathway or with a relevant biological function or disease, according to the IPA database library. The Ingenuity® Upstream Regulator Analysis computed an activation *z*-score and a Fisher's exact *p*-value (overlap *p*-value) for the most altered genes. Furthermore, we used the IPA Upstream Regulator application to assemble an interactome using the five upstream regulators with the highest activation *z*-scores and the five upstream regulators with the lowest activation *z*-scores, along with the corresponding downstream target genes/molecules whose expression was significantly altered in the CP of J20 mice at each age. To be included in the interactome, the networks had to present at least one connection with an upstream regulator or with a downstream gene of a different adjacent network; orphan networks were not presented.

2.6. Primary cultures of CP epithelial cells and incubation with $A\beta_{1-42}$

Primary cultures of CP epithelial cells were prepared from the CP tissue of rat pups due to the higher cellular yield of the isolation procedure when compared to the mouse CP. This procedure was performed as described before (Marques et al., 2009), with minor modifications. Briefly, neonates (P5–P7) were sacrificed and the CP dissected from the four brain ventricles, under a conventional light stereomicroscope (SZX7, Olympus). The tissue was rinsed in phosphate buffer saline (PBS, Invitrogen, Carlsbad, CA, USA) without Ca^{2+} and Mg^{2+}, followed by a 25 min digestion with 0.1 mg/mL pronase (Sigma–Aldrich, St. Louis, MO, USA) at 37 °C. Predigested tissue was recovered by sedimentation and briefly shaken in 0.025% trypsin–EDTA (Invitrogen) containing 12.5 μg/ml DNAse I (Roche, Amadora, Portugal). The supernatant was then withdrawn and kept on ice with 10% fetal bovine serum (FBS, Invitrogen). This step was repeated five times. Cells were collected by centrifugation and re-suspended in culture media consisting of Ham's F-12 and Dulbecco's modified Eagle's medium (DMEM-F12, Invitrogen) supplemented with 10% FBS, 2 mM glutamine, 50 mg/mL gentamycin, 5 mg/mL insulin, 5 mg/mL transferrin, 5 ng/mL sodium selenite, 10 ng/mL epidermal growth factor, 2 mg/mL hydrocortisone and 5 ng/mL basic fibroblast growth factor (all from Sigma–Aldrich). For further enrichment, cells were incubated on plastic dishes for 2 h at 37 °C. The supernatant containing the CP epithelial cells was collected and placed for seeding on 0.4 μm pore size transwells (Corning Life Sciences, Lowell, MA, USA) coated with laminin (BD Biosciences, Bedford, MA, USA) at a density of 1×10^5 cells/cm^2. The culture medium was changed every two days and CP epithelial cells were maintained in culture for 5–7 days, at 37 °C in a humid atmosphere (5% CO_2), before performing the experiment. To assess the cellular purity and confluence after 7 days in culture, an immunofluorescent staining was performed, using a primary antibody for transthyretin (TTR) (kindly provided by Dr. Maria Joao Saraiva, Institute for Molecular and Cell Biology, Porto, Portugal), a specific marker of CP epithelial cells (Sousa et al., 2007). Cell counting revealed that $\geqslant 95\%$ of the cells stained positive for TTR. Stock $A\beta_{1-42}$ (American Peptide Company, Sunnyvale, CA, USA) was prepared by dissolving the peptides in Tris–NaCl buffer (150 mM NaCl and 50 mM Tris–HCl pH 7.4, all from Sigma–Aldrich) to a final concentration of 221.5 μM and kept at −80 °C. After reaching confluence, CP epithelial cells were incubated for 60 h with DMEM-F12 alone (vehicle) or a solution of 1 μM monomeric/dimeric $A\beta_{1-42}$, by dissolving stock $A\beta_{1-42}$ in DMEM-F12 medium.

2.7. Primary cultures of astrocytes and neurons

This procedure was performed as described before (Mesquita et al., 2014). Details are provided in Supplementary methods (Appendix A).

2.8. Gene expression analysis by qRT-PCR

The quality assessment and quantification of the total RNA extracted from CP samples was performed in the NanoDrop® ND-1000 and 350 ng of RNA from each sample were amplified using the MessageAmp™ II aRNA Amplification Kit (Ambion, Carlsbad, CA, USA) according to the manufacturer's instructions. Total RNA was also extracted from primary cultures of CP epithelial cells, using the RNeasy® Plus Micro Kit (Qiagen), or from samples of dHPC, using the Trizol reagent (Invitrogen), following the manufacturer's instructions. Then, after quantification in the NanoDrop®, 500 ng of total or amplified RNA from each sample was reverse transcribed into cDNA using the iScript™ cDNA Synthesis Kit (Bio-Rad Laboratories, Hercules, CA, USA) following the manufacturer's instructions. Primers used to measure the expression levels of selected mRNA transcripts by qRT-PCR were designed using the Primer-BLAST tool of the National Center for Biotechnology Information (Bethesda, MD, USA) on the basis of the respective GenBank accession numbers. The reference gene hypoxanthine guanine phosphoribosyl transferase (*Hprt*) was used as internal standard for the normalization of the expression of selected transcripts. All GenBank accession numbers for *Mus musculus* (*in vivo* studies) or *Rattus norvegicus* (*in vitro* experiments) gene transcripts and primer DNA sequences are provided in Supplementary data (Appendix A). Annealing temperatures are available on request. The qRT-PCR was performed on a CFX 96TM real-time system instrument (Bio-Rad), with the SsoFast™ EvaGreen® Supermix (Bio-Rad) according to the manufacturer's instructions, using equal amounts of cDNA from each sample. The cycling parameters were

1 cycle at 95 °C for 15 min, followed by 40 cycles at 94 °C for 15 s, annealing temperature (primer specific) for 30 s and 72 °C for 30 s, finishing with 1 cycle at 65 °C to 95 °C for 5 s (melting curve). Product fluorescence was detected at the end of each elongation cycle. All melting curves exhibited a single sharp peak at the expected temperature.

2.9. Quantification of Aβ and IFN-α in the CSF

The quantification of Aβ in the CSF was performed by a direct enzyme-linked immunosorbent assay (ELISA) performed in Nunc MaxiSorp® flat-bottom 96-well plates (ThermoFisher Scientific). The wells were coated with 1 μL of CSF diluted in 99 μL of a KH_2PO_4/K_2HPO_4 buffer (pH 8.0) solution (1:100 dilution factor), for 2 h at 37 °C. After washing with PBS 0.05% Tween® 20 (Sigma–Aldrich), a blocking step with PBS 10% skim milk (Nestle S.A., Linda-a-Velha, Portugal) was performed for 1 h at room-temperature (RT). Then, consecutive incubations for 1 h at RT were performed: first with rabbit anti-human Aβ (1:500, D54D2, Cell Signaling Technology, Danvers, MA, USA), second with biotinylated horse anti-rabbit (1:500, Vector Laboratories, Burlingame, CA, USA) and third with streptavidin-horseradish peroxidase (1:2500, Sigma–Aldrich). Each incubation step was separated by thorough washes with PBS 0.05% Tween® 20 and PBS. Finally, the detection of Aβ was achieved by adding a solution containing 2,2′-azino-bis(3-ethylbenzothiazoline-6-sulfonic acid) diammonium salt (ABTS, Sigma–Aldrich), which induced a colorimetric reaction read at 405 nm. The standard curve was obtained using known concentrations of human $Aβ_{1–42}$ (American Peptide Company, Sunnyvale, CA, USA) that ranged from 0.1 to 100 ng/μL (considering the linearity of the assay). The levels of IFN-α were measured in 1 μL of CSF, using the commercially available Mouse IFN alpha Platinum ELISA kit (Affymetrix, eBioscience, Vienna, Austria), according to the manufacturer's instructions. The standard curve was obtained using known concentrations of mouse IFN-α that ranged from 31.3 to 2000 pg/mL.

2.10. Immunofluorescent staining for Aβ peptides

Serial sections of frozen brain (coronal sections) with a thickness of 20 μm were cut in the cryostat and collected to SuperFrost® Plus slides (ThermoFisher Scientific). Sections were then fixed for 20 min in 4% PFA (Panreac), at RT. A step of antigen retrieval was performed afterwards, by heating the tissue sections for 20 min in 10 mM, pH 6.0, acetic acid (Sigma–Aldrich). After a blocking step for 1 h at RT, with a solution of 0.5% bovine serum albumin (BSA, Sigma–Aldrich) in PBS 0.3% Triton X-100 (Sigma–Aldrich) (PBS-T), the tissue sections were incubated, overnight, with the primary antibody rabbit anti-human Aβ (1:1000, D54D2, Cell Signaling) diluted in blocking solution. After this period, the sections were rinsed in PBS-T and incubated with a secondary antibody conjugated to Alexa-594 (1:500, Invitrogen) diluted in PBS-T for 1 h at RT. Finally, after incubation in a solution of 4,6-diamidino-2-phenylindole (DAPI, 1:1000, Invitrogen) in PBS for 5 min at RT, the sections were washed with PBS, and mounted in Shandon Immu-Mount (ThermoFisher Scientific). Fluorescence analysis and image capture were performed using a conventional fluorescence microscope (BX61; Olympus).

2.11. Immunohistochemistry for glial fibrillary acidic protein (GFAP) and ionized calcium-binding adapter molecule 1 (IBA1)

To assess the morphology of astrocytes and the number of microglia/macrophages from the DG of the dHPC, 10 μm thick coronal brain sections were deparaffinized and antigen retrieval was performed by heating the tissue sections for 20 min in 10 mM acetic acid solution, pH 6.0 (Sigma–Aldrich). Next, tissue peroxidases were inactivated, by immersion in a 0.3% H_2O_2 solution for 30 min, and a blocking step was performed by incubation in a PBS-T 0.5% BSA solution. Sections were later incubated overnight, at RT, with rabbit anti-mouse GFAP (1:200, Dako, Golstrup, Denmark) or rabbit anti-mouse IBA1 (1:300, Wako Chemicals GmbH, Neuss, Germany) antibodies diluted in blocking solution and, in the following day, rinsed in PBS-T and incubated with biotinylated goat polyvalent antibody (UltraVision Large Volume Detection System, ThermoFisher Scientific) for 1 h at RT. Finally, after rinsing in PBS-T, sections were further incubated for 1 h with streptavidin- horseradish peroxidase (UltraVision, ThermoFisher Scientific), rinsed again in PBS and exposed to a 3,3-diaminobenzidine solution (Sigma–Aldrich) for 10 min. After a thorough wash with PBS, sections were dried and mounted in Entellan (Merck, Darmstadt, Germany). The morphology of 10 astrocytes ($GFAP^+$ cells) located in the DG of the dHPC of each mouse ($N = 30$ astrocytes/group) was assessed using an optical microscope (BX51TF, Olympus) coupled to a camera (U-TV1X-2, Olympus) and with the NeuroLucida software (Olympus). The samples were given a code name so that the morphology could be assessed by an investigator who was blinded to the experiment. Data was analyzed with the NeuroExplorer software (Olympus). The number of microglia/macrophages in the DG of the dHPC was assessed in serial brain sections and the number of cells per mm^2 was calculated ($N = 4$/group at 3 and 5–6 months, and $N = 5$/group at 11–12 months).

2.12. Statistical analysis

Values are reported as mean ± standard error of mean (SEM). The number of biological replicates (N) of the representative independent experiments is specified in the legend of each figure. Statistical significant differences between groups were determined using the parametric repeated measures two-way ANOVA with Bonferroni post hoc test (two-tailed) or the non-parametric two-tailed Mann Whitney test and Kruskal–Wallis with Dunns' multiple comparison test (two-tailed). Values were considered to be statistically significant for $p < 0.05$ (*), $p < 0.01$ (**) and $p < 0.001$ (***). Simple correlations were obtained by regression analysis, using the Pearson's correlation test, and results were considered to be statistically significant for $p < 0.05$ (two-tailed). Regression models (two-tailed) were designed and run in Matlab R2009b (7.9.0.529, Mathworks, Natick, MA, USA). To avoid collinearity, the independent variables age and IFN-α were centered, considering for that the respective mean values. To verify the statistical significance of the interactions between the different predictors, four interaction terms were created (age*genotype, age*IFN-α, genotype*IFN-α and age*genotype*IFN-α). No animals were excluded from the analysis.

3. Results

3.1. Age-associated memory decline was anticipated in J20 mice

The MWM was used to test the performance of WT and J20 mice in a spatial reference-memory task at 3, 5–6 and 11–12 months of age (Fig. 1A and B). At 3 months, WT mice took significantly less time to find the hidden platform, when compared to age-matched J20 mice (Fig. 1B). At the ages of 5–6 months and 11–12 months, the differences between WT and J20 mice became smaller; still, at 11–12 months, J20 mice presented a significantly worst performance than WT mice at day 5 of the MWM (Fig. 1B). No statistical significant differences were observed in terms of swimming speed in the MWM, when comparing mice of different

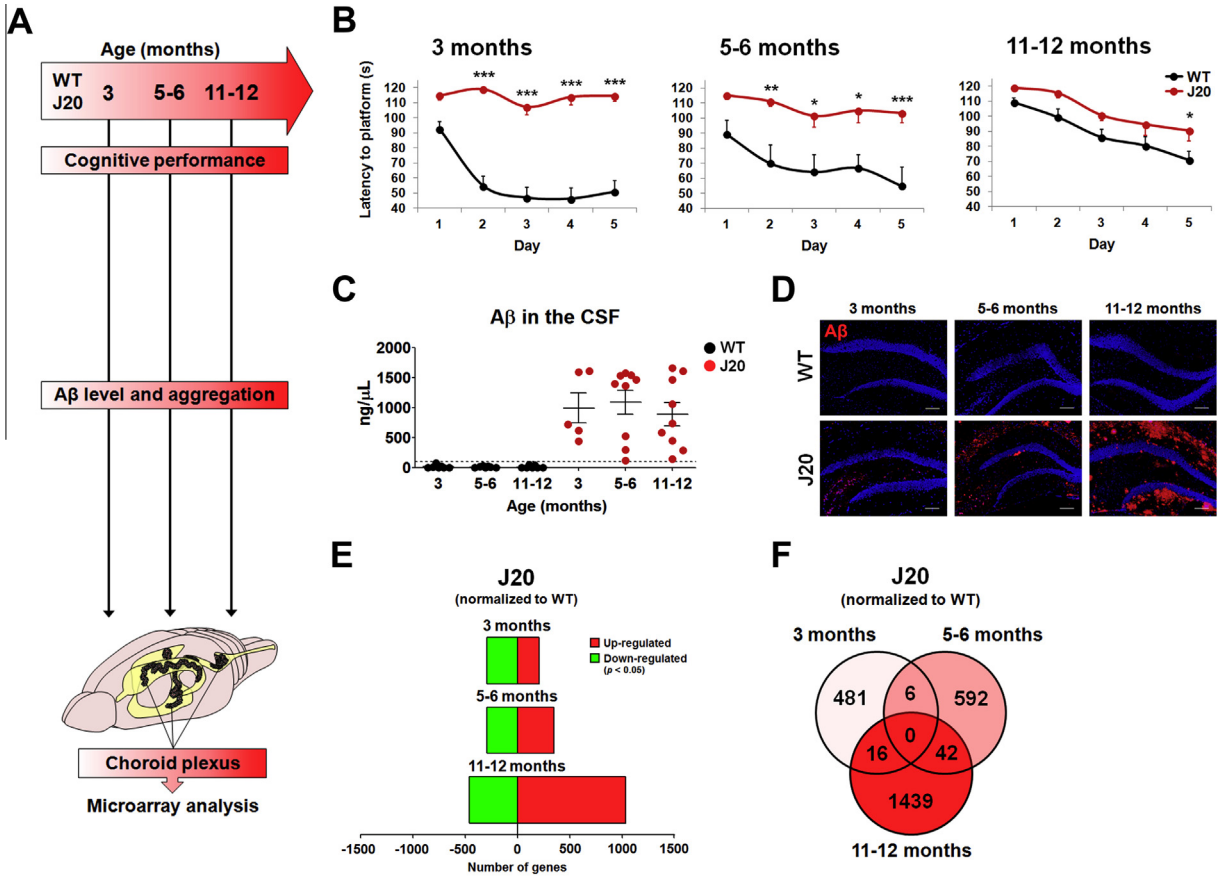

Fig. 1. Cognitive performance, Aβ pathology and microarray analysis of the CP of WT and J20 mice at 3, 5–6 and 11–12 months. (A) Cognitive performance and the level and state of aggregation of Aβ peptides were assessed in the brain of male WT and J20 mice, at the ages of 3, 5–6, 11–12 months. RNA was isolated and purified from samples of CP extracted from all the brain ventricles of each WT or J20 mice. RNA samples from the CP of WT mice at 3 ($N = 3$), 5–6 ($N = 4$) and 11–12 ($N = 6$) months, and of J20 mice at 3 ($N = 4$), 5–6 ($N = 4$) and 11–12 ($N = 3$) months were used to analyze the transcriptomic changes by microarray. (B) Assessment of the performance in the MWM during the light phase of the diurnal cycle, showed that J20 mice present a severe impairment in spatial reference-memory already at 3 months, when compared to age-matched WT mice; however, the differences between WT and J20 mice in the MWM test are lessen at 5–6 and at 11–12 months, mostly due to the worst performance of WT mice at these ages. (C) The level of Aβ was measured in CSF samples from WT and J20 mice; no differences were found between the levels of Aβ measured in the CSF of J20 mice at different ages. (D) Staining for Aβ in the dHPC revealed, in J20 mice only, an initial staining predominantly in the CA3 region, at 3 months, and a progressive increase in the level and degree of extracellular aggregation of Aβ peptides with aging, mostly in the molecular layer of the dHPC. (E) The number of significantly ($p < 0.05$) up-(red) and down-regulated (green) genes in the CP of J20 mice was obtained by normalizing to the expression levels of the corresponding genes in the CP of age-matched WT mice. There was an age-dependent increase in the number of genes whose expression was significantly altered in the CP of J20 mice. (F) After comparing the significantly altered genes in the CP of J20 at 3 vs 5–6 months, at 5–6 vs 11–12 months and at 3 vs 11–12 months, we found a common expression of 6, 42 and 16 genes, respectively; however, we found no commonly altered genes after overlapping the CP transcriptomic changes of J20 mice at 3, 5–6 and 11–12 months. Results are presented as mean ± SEM [at 3 months, N (WT) = 16 and N (J20) = 8; at 5–6 months, N (WT) = 8 and N (J20) = 10; at 11–12 months, N (WT) = 23 and N (J20) = 15] in (B); $^{*}p < 0.05$, $^{**}p < 0.01$ and $^{***}p < 0.001$; Repeated measures two-way ANOVA, with Bonferroni post hoc test (two-tailed). Results are presented as mean ± SEM [at 3 months, N (WT) = 7 and N (J20) = 5; at 5–6 months, N (WT) = 7 and N (J20) = 9; at 11–12 months, N (WT) = 7 and N (J20) = 9] in (C); Kruskal–Wallis with Dunns' multiple comparison test (two-tailed). Scale bars indicate 100 μm in (D).

genotypes at each age (Supplementary Fig. 1). To assess brain amyloid pathology in J20 mice, we measured the levels of Aβ in the CSF and evaluated the degree of Aβ aggregation and deposition in the dHPC (Fig. 1C and D). There were no statistically significant differences between the levels of Aβ in the CSF of J20 mice at different ages (Fig. 1C); yet, there was a progressive accumulation of Aβ and increased plaque burden in the dHPC of J20 mice with aging that was more obvious at 11–12 months (Fig. 1D). No Aβ was detected in the CSF or in the brain of WT mice (Fig. 1C and D).

3.2. Age and Aβ impacted differently on the CP transcriptome of WT and of J20 mice

The changes in the CP transcriptome of J20 mice were assessed by microarray at 3, 5–6 and 11–12 months of age and normalized to the changes observed in age-matched WT mice (Fig. 1A). The highest number of up- and down-regulated genes in the CP of J20 mice was observed at 11–12 months (Fig. 1E). Of notice, we found no commonly altered genes after overlapping the CP transcriptomic changes of J20 mice at 3, 5–6 and 11–12 months (Fig. 1F). Moreover, we found few commonly altered genes when comparing the transcriptomic changes in the CP of J20 mice two ages at a time (Fig. 1F). The ten most up- or down-regulated genes in the CP of J20 mice (Table 1) revealed alterations in genes that are involved in the functions classically attributed to the CP, such as the modulation of the CSF's composition, and that regulate the survival of CP cells and the maintenance of the barrier integrity (Table 1). We also analyzed the effect of aging, *per se*, in the CP transcriptome, by normalizing the changes observed in WT or J20 mice at 11–12 months to that of 3 months-old mice of the same genotype (Supplementary Figs. 2 and 3). Interestingly, we found a consistent alteration in the expression of genes that regulate the cellular circadian rhythm in the 11–12 months-old mice, which is describe in detail in the Supplementary data (Supplementary Figs. 2 and 3 and Supplementary Tables 1 and 2). Surprisingly, when considering all the analyzed data sets and comparisons

Table 1
Most altered genes in the CP of J20 mice (normalized to age-matched littermate WT mice).

Up-regulated genes					Down-regulated genes				
Accession number	Entrez Gene name (*Mus musculus*)	Gene symbol	Fold change	*p*-value	Accession number	Entrez Gene name (*Mus musculus*)	Gene symbol	Fold change	*p*-value
3 months (J20 vs WT)									
NM_011638.3	Transferrin receptor	*Tfrc*	1.64	0.007	NM_011066.1	Period circadian clock 2	*Per2*	−1.52	0.019
NM_011909.1	Ubiquitin specific peptidase 18	*Usp18*	1.43	0.017	NM_001033302.1	Circadian associated repressor of transcription	*Ciart*	−1.38	0.024
NM_019498.1	Olfactomedin 1	*Olfm1*	1.33	0.011	NM_008504.2	Granzyme M (lymphocyte met−ase 1)	*Gzmm*	−1.36	0.027
NM_008728.2	Natriuretic peptide receptor 3	*Npr3*	1.32	0.001	NM_015750.1	Sialidase 2 (cytosolic sialidase)	*Neu2*	−1.33	0.038
NM_011819.1	Growth differentiation factor 15	*Gdf15*	1.32	0.026	NM_053147.2	Prostaglandin I2 (prostacyclin) synthase	*Ptgis*	−1.31	0.021
NM_001039086.1	Rap guanine nucleotide exchange factor (GEF) 1	*Rapgef1*	1.28	0.007	NM_008968.2	TSC22 domain family, member 3	*Tsc22d3*	−1.30	0.012
NM_013769.1	Tight junction protein 3	*Tjp3*	1.24	0.038	NM_001077364.1	DEAD (Asp-Glu-Ala-Asp) box helicase 17	*Ddx17*	−1.30	0.044
NM_009423.2	Tnf receptor-associated factor 4	*Traf4*	1.22	0.014	NM_148941.1	ELOVL fatty acid elongase 4	*Elovl4*	−1.29	0.009
NM_020278.2	Leucine-rich, glioma inactivated 1	*Lgi1*	1.21	0.025	NM_011072.2	Profilin 1	*Pfn1*	−1.24	0.039
NM_138314.1	NME/NM23 family member 7	*Nme7*	1.21	0.049	XM_354652	3-hydroxyanthranilate 3,4-dioxygenase	*Haao*	−1.25	0.021
5–6 months (J20 vs WT)									
NM_033373.1	Keratin 23 (histone deacetylase inducible)	*Krt23*	1.48	0.008	NM_198110.1	Guanine nucleotide binding protein-like 3 (nucleolar)-like	*Gnl3l*	−1.46	0.028
NM_021389.3	SH3-domain kinase binding protein 1	*Sh3kbp1*	1.37	0.011	NM_007751.1	Cytochrome c oxidase subunit VIIIb	*Cox8b*	−1.44	0.007
NM_010789.1	Meis homeobox 1	*Meis1*	1.32	0.008	NM_011213.1	Protein tyrosine phosphatase, receptor type, F	*Ptprf*	−1.30	0.012
NM_138955.2	ATP-binding cassette, sub-family G (WHITE), member 4	*Abcg4*	1.29	0.010	NM_010024.1	Dopachrome tautomerase	*Dct*	−1.30	0.006
NM_021399	B-cell CLL/lymphoma 11B (zinc finger protein)	*Bcl11b*	1.29	0.041	NM_053110.2	Glycoprotein (transmembrane) nmb	*Gpnmb*	−1.26	0.042
NM_024440.1	Derlin 3	*Derl3*	1.26	0.005	NM_028756.2	Solute carrier family 35, member A5	*Slc35a5*	−1.26	0.005
NM_021391.2	Protein phosphatase 1, regulatory (inhibitor) subunit 1A	*Ppp1r1a*	1.26	0.040	NM_026002	Metadherin	*Mtdh*	−1.25	0.022
NM_011807	Discs, large homolog 2 (Drosophila)	*Dlg2*	1.25	0.037	NM_133995.1	Ureidopropionase, beta	*Upb1*	−1.21	0.006
NM_007669.2	Cyclin-dependent kinase inhibitor 1A (p21, Cip1)	*Cdkn1a*	1.24	0.047	NM_023805.2	Solute carrier family 38, member 3	*Slc38a3*	−1.20	0.031
NM_010630.1	Kinesin family member C2	*Kifc2*	1.23	0.033	NM_145979.1	Chromodomain helicase DNA binding protein 4	*Chd4*	−1.20	0.045
11–12 months (J20 vs WT)									
NM_007393.1	Actin beta	*Actb*	2.30	0.033	NM_008786.1	Protein-L-isoaspartate (D-aspartate) O-methyltransferase 1	*Pcmt1*	−1.84	0.048
NM_198110.1	Guanine nucleotide binding protein-like 3 (nucleolar)-like	*Gnl3l*	1.95	<0.001	NM_009842.3	CD151 molecule (Raph blood group)	*Cd151*	−1.68	0.036
NM_001081642.1	X-linked lymphocyte-regulated 4A	*Xlr4a*	1.76	0.023	NM_022331.1	Homocysteine-inducible, endoplasmic reticulum stress-inducible, ubiquitin-like domain member 1	*Herpud1*	−1.61	0.019
NM_145470.2	DEP domain containing MTOR-interacting protein	*Deptor*	1.53	0.024	NM_012002.1	COP9 signalosome subunit 6	*Cops6*	−1.60	0.021
NM_133903.2	Spondin 2, extracellular matrix protein	*Spon2*	1.51	0.016	NM_183187.2	Family with sequence similarity 107, member A	*Fam107a*	−1.58	0.014
XM_196324.2	Deafness, autosomal recessive 31	*Dfnb31*	1.47	0.005	NM_007472.1	Aquaporin 1 (Colton blood group)	*Aqp1*	−1.52	0.028
NM_054071.1	Fibroblast growth factor receptor-like 1	*Fgfrl1*	1.47	0.012	NM_008947	Proteasome (prosome, macropain) 26S subunit, ATPase, 1	*Psmc1*	−1.52	0.012
NM_013882.1	G-2 and S-phase expressed 1	*Gtse1*	1.46	0.004	NM_008610.1	Matrix metallopeptidase 2 (gelatinase A)	*Mmp2*	−1.50	0.008
NM_016972.2	Solute carrier family 7, member 8	*Slc7a8*	1.44	0.008	NM_007413.2	Adenosine A2b receptor	*Adora2b*	−1.50	0.047
NM_001080126.1	Caspase 8, apoptosis-related cysteine peptidase	*Casp8*	1.43	0.031	NM_008504.2	Granzyme M (lymphocyte metase 1)	*Gzmm*	−1.49	0.003

performed, the fold-changes in gene expression are small and varied to a maximum fold-increase of 3.01 and fold-decrease of 3.45 (Table 1 and Supplementary Tables 1 and 2).

3.3. The pattern of changes in the CP transcriptome of J20 mice varied with age

Using the gene network analysis computed by the IPA software, we were able to establish a list of the 5 most altered gene networks, and associated biological functions, at each age in the CP of J20 mice (Fig. 2A–F). Of notice, this analysis revealed that the most altered gene network is different at each age (Fig. 2B, D and F). At 3 months, at least two of the altered gene networks were involved in the regulation of one of the following biological functions: molecular transport, metabolism of small molecules, cell-to-cell signaling/endocrine system function and cell death/survival (Fig. 2A). At 5–6 months of age, in addition to the alterations in the genes of network 5 (Fig. 2C) already affected at 3 months (Fig. 2A), the main biological functions and processes found to be altered were related with the hematological system, inflammatory and humoral immune responses and cellular morphology and motility (gene networks 1–4, Fig. 2C). Of notice, those alterations in inflammation/immune-related pathways at 5–6 months were sustained at 11–12 months, since the most altered gene network in the CP of 11–12 months-old J20 mice regulated the inflammatory and antimicrobial responses (gene network 1, Fig. 2E) and included, as central modulators, the genes interferon beta 1 (*Ifnb1*) and signal transducer and activator of transcription 1 (*Stat1*) (Fig. 2F). The gene networks 2–5, affected at 11–12 months, showed again alterations in processes such as small molecule biochemistry, molecular transport and cellular signaling, movement and survival (Fig. 2E).

3.4. Type I and II IFN responses were altered in the CP of J20 mice

Taking into account the previous alterations, particularly those regarding gene pathways involved in the regulation of the inflammatory/immune responses in the CP of J20, we next pursued the underlying transcriptional regulators that could be responsible for such alterations in gene expression (Fig. 3 and Supplementary Table 3). For that analysis, we used the IPA Upstream Regulator application, that computed an activation *z*-score predictive of the activation status of a given transcriptional regulator, taking into account the expression level of the corresponding downstream target genes in the CP of J20 mice at each age (Fig. 3A). Using the five regulators with highest *z*-score and the five regulators with lowest *z*-score (Supplementary Table 3), this analysis allowed the assembly of gene interactomes (Fig. 3B–D). At 3 months, this approach discriminated the genes Toll-like receptor 9 (*Tlr9*), interferon regulatory factor 7 (*Irf7*) and interferon (alpha and beta) receptor 1 (*Ifnar1*), all of them predicted to be up-regulated in the CP of J20 mice, when compared with age matched WT mice (Fig. 3A and B). Surprisingly, at the ages of 5–6 and 11–12 months, interferon gamma (*Ifng*) presented a low activation *z*-score that suggested a possible down-regulation of this gene in the CP of J20 mice (Fig. 3A, C and D). Noticeably, the inactivation of the *Ifng*-regulated pathway was predicted to affect the expression of 18 target genes at 5–6 months (Fig. 3C and Supplementary Table 3), an effect that was even more marked at 11–12 months, affecting 25 downstream genes/molecules (Fig. 3D and Supplementary Table 3).

To confirm and complement the array data, the expression of type I IFN-related genes [*Tlr9*, *Ifnar1*, *Irf7*, interferon alpha 1 (*Ifna1*) and interferon beta 1 (*Ifnb1*)] and of type II IFN-related genes [*Ifng* and intercellular adhesion molecule 1 (*Icam1*)] was measured by qRT-PCR (Fig. 4A–G). Once again, we observed an overexpression of *Tlr9*, *Ifnar1*, *Irf7* and *Ifnb1*, in the CP of J20 mice at 3 months, when compared with WT mice; together with *Ifna1*, these genes remained highly expressed in the CP of J20 mice at 5–6 months when compared to 3 months-old WT mice (Fig. 4A–E). In the CP of WT mice, despite the unaltered expression of *Irf7*, *Ifna* and *Ifnb1* (Fig. 4C–E) at different ages, we observed a significant overexpression of *Tlr9* and *Ifnar1* at 11–12 months, when compared to the 3 months-old mice of the same genotype (Fig. 4A and B). The genes *Ifng* and *Icam1*, which are related with a type II IFN response, were also significantly overexpressed at 3 months in the CP of J20 mice, when compared to age-matched WT mice (Fig. 4F and G). On the other hand, at 5–6 months, there was a significant down-regulation of *Ifng* in the CP of J20 mice, when compared to the expression levels at 3 months in J20 and at 5–6 months in WT mice, which was maintained at 11–12 months (Fig. 4F).

Next, to discriminate the specific contribution of CP epithelial cells to the expression of type I or type II IFN genes in AD, we performed primary cultures of CP epithelial cells on a transwell system (to mimic the *in vivo* tight and polarized arrangement that these epithelial cells present in the blood–CSF barrier, Fig. 4H), and stimulated these cells at the apical membrane, which mimics the CSF-side, with 1 μM $A\beta_{1-42}$. We observed that in response to $A\beta_{1-42}$, the CP epithelial cells significantly overexpressed the type I IFN genes *Tlr9* and *Ifna1*, but not the type II IFN gene *Ifng* (Fig. 5I–K).

3.5. Aging altered the pattern of type I and II IFN gene expression in the dHPC of WT and of J20 mice

To further investigate the IFN response at the brain parenchyma, we measured the expression of the same type I and II IFN genes in the dHPC of WT and J20 mice at different ages (Fig. 5A–G). As observed before in the CP of J20 mice, there was an

Table 2
Main effects of age, genotype and IFN-α levels in the CSF, alone (model 1) and taking into account the interactions between independent variables (model 2), as predictors of the latency to platform in the MWM test.

Independent variables and interactions	Latency (model 1)			Latency (model 2)		
	β	*p*	R^2 (adjusted)	*β*	*p*	R^2 (adjusted)
Age	2.5840	0.3372	0.6712	1.7302	0.5006	0.7177
Genotype	36.853	<0.0001		35.962	<0.0001	
IFN-α	0.8746	0.0087		0.4878	0.2056	
Age*Genotype	Not included			−15.595	0.0038	
Age*IFN-α				−0.0957	0.8435	
Genotype*IFN-α				−0.2905	0.7038	
Age*Genotype*IFN-α				0.3214	0.7405	

WT mice: *N* (3 months) = 12; *N* (5–6 months) = 7; *N* (11–12 months) = 9.
J20 mice: *N* (3 months) = 5; *N* (5–6 months) = 9; *N* (11–12 months) = 8.
No collinearity was observed between independent variables.

A **Gene expression alterations in 3 months-old J20 mice (normalized to 3 months-old WT mice)**

Top 5 Networks/Functions	Number of genes	Up-regulated molecules	Down-regulated molecules
1 Endocrine System Development and Function, Molecular Transport, Small Molecule Biochemistry	9↑ 20↓	HTR2C, Il3, LIPE, NKX2-2, NR3C1, RUNX2, SIRT6, SMARCC1, SS18L1	ABCC8, ACADL, C5, CCR4, CD79B, CTSE, DOK1, ERK, HMGA1, Ins1, ITGB1BP2, MAPK12, Ms4a4b(includes others), PASK, Prl3d1(includes others), SLC38A1, SLC6A19, TBC1D4, TRIB3, TSC22D3
2 Cell Death and Survival, Organismal Development, Cellular Development	9↑ 17↓	AP2A1, DSG1, ISG15, MED1, MST1R, SCGB1A1, TFRC, TNFSF12, USP18	BBC3, CFD, DLG1, HOXA9, ICOS, IL2RB, KDR, Map3k7, PER2, PFN1, PLCG1, RPSA, SKP2, STAM2, TBX21, TNFAIP8L2, UCP1
3 Organismal Injury and Abnormalities, Cell-To-Cell Signaling and Interaction, Small Molecule Biochemistry	9↑ 9↓	ABLIM1, ABR, CYBRD1, DENND2D, GPC4, IPCEF1, LGI1, PRSS2, WISP1	CANT1, CPNE7,HIST1H1T, HTR2A, MAST1, RCN1, STOM, TEAD1, TFAP2B
4 Cell Death and Survival, Connective Tissue Disorders, Hematological Disease	7↑ 10↓	ACSM3, CELA3B, Cyp2j5, KIFC2, KLK3, Slco1a1, TM4SF4	AOX1, ATF7, C5, C8A, ELOVL4, GOLT1A, KNG1, TBX21, TMED6, UGT2B7
5 Carbohydrate Metabolism, Molecular Transport, Small Molecule Biochemistry	9↑ 8↓	APBB3, CPSF1, EPB41L2, MBD1, OTOF, RAPGEF1, SIRT6, TFAP2C, TMCC2	ACADL, ARL2BP, AUTS2, CRAT, NEU2, Olfr1107, SKP2, ST18

↑ up-regulated; ↓ down-regulated

B **3 months Network 1 (most altered)**

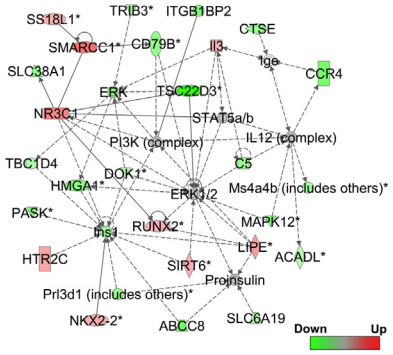

C **Gene expression alterations in 5-6 months-old J20 mice (normalized to 5-6 months-old WT mice)**

Top 5 Networks/Functions	Number of genes	Up-regulated molecules	Down-regulated molecules
1 Gastrointestinal Disease, Neurological Disease, Hematological System Development and Function	19↑ 13↓	Cdkn1c, CEBPA, FKBP4, GABRD, GAPDH, GCAT, HAPLN3, HDAC5, MBTPS1, Meis1, NR1I2, OTOF, PHLDA3, RASGRP2, SH3KBP1, SLC2A1, SP6, TMCC2, USP9X	APOC2, CEACAM1, COCH, FASN, HTT, IL5, LRRC8C, MED1, MTDH, PRKAG3, SLC39A8, SYT7, UPB1
2 Cell Morphology, Cellular Movement, Hematological System Development and Function	14↑ 13↓	AIRE, CSRP3, EGFR, IGFBP2, ITGA3, LILRB3, MAPK12, MMP8, MSR1, NAB2, RTN4R, SARM1, SOX4, UCP2	ANGPT1, CREB1, DGKI, DNM1, ETV5, GTF2F2, HSPA4, JAM2, SPI1, TLN1, UBD, WISP1, WNT1
3 Protein Synthesis, Inflammatory Response, Cellular Movement	18↑ 8↓	AK3, BCL11B, CASP7, CRH, CXCR2, CYP3A5, FEZF2, HLA-A, ISG20, KCNIP2, KRT17, MPO, MYD88, OLFM4, PER2, PPP1R1A, Tcf7, TRAF6	CASP4, Casp12, FURIN, IL2RA, MARCO, MUC5AC, PTPN11, ZNF274
4 Hematological System Development and Function, Humoral Immune Response, Tissue Morphology	12↑ 11↓	ABL1, BLM, CD22, DSCAM, FLT3, GHRH, IGF1, IL5RA, PDCD1, PROKR1, RASGRP1, SH2B2	AMH, CDH2, FOXL2, FUT8, HSD17B3, KLRB1, MAFA, NLRP5, PTPRF, SFN, SPPL2A
5 Endocrine System Development and Function, Small Molecule Biochemistry, Lipid Metabolism	7↑ 12↓	CASP14, FUT9, GRIA3, IL22RA2, MTRR, PIH1D3, Speer4a(includes others)	ACOT2, B3GALT1, CLCA1, CYB5B, Cyp2c54(includes others), FOXF1, GML, Hsd3b4(includes others), NSDHL, RDH16, SLC23A1, Ssty1(includes others)

↑ up-regulated; ↓ down-regulated

D **5-6 months Network 1 (most altered)**

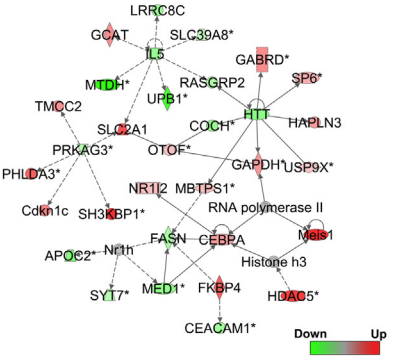

E **Gene expression alterations in 11-12 months-old J20 mice (normalized to 11-12 months-old WT mice)**

Top 5 Networks/Functions	Number of genes	Up-regulated molecules	Down-regulated molecules
1 Protein Synthesis, Antimicrobial Response, Inflammatory Response	24↑ 9↓	ANKRD17, CDCA3, CLSTN1, CYP2C8, EGR3, FGL2, FLT3, IFN alpha/beta, IFNB1, NAB1, Oas1b, PLXND1, Retnla, RILPL1, SCGB3A2, SLFN13, SMO, STARD4, STAT1, TNFAIP2, TRIM25, USP21, VIPR1, ZFP64	CASP4, FKBP9, GBP3, IFNGR2, Irgm1, MEX3C, SAMSN1, TK1, UNC13D
2 Cellular Response to Therapeutics, Cell Death and Survival, Cell Morphology	12↑ 18↓	ATM, BAX, BBC3, BLM, BMF, CHRNA3, DMTF1, FOXJ1, IL1RAP, MAPK10, PELI1, TXN	ACP2, BID, CLEC4E, ENPEP, FANCG, IFIH1, IL36G, KEAP1, MCM8, ORA1, PGC, PRMT2, RAD51, STIM1, TANK, VTN, Wfdc17, XBP1
3 Cell Signaling, Molecular Transport, Small Molecule Biochemistry	22↑ 8↓	CD19, CD81, Cux1, DKK2, GPER1, HNRNPAB, IGF1, ITGA3, MAPK12, MARCKSL1, MST1, OGN, PLEC, SBSN, SLC22A2, SPP1, SPRED2, SYNE3, TAS1R3, TBX6, VCAN, VCL	AGT, GABBR1, GNA11, HERPUD1, P2RX7, SEL1L, SLC22A5, VNN1
4 Carbohydrate Metabolism, Molecular Transport, Small Molecule Biochemistry	20↑ 10↓	APOA5, CDKN2B, COX7B, DMP1, GCLM, GHSR, IRS1, LEFTY1, NRF1, PCSK2, PNLIPRP1, PNPLA2, RAB9A, RFX4, RNF111, SH2B1, SLC9B2, SLIT3, TPP2, TPT1	C8orf44-SGK3/SGK3, COL7A1, FFAR4, FGF1, FHL1, FLCN, LCAT, PMEPA1, RHOU, SERPINE1
5 Organismal Survival, Tissue Morphology, Cellular Movement	19↑ 9↓	APBA3, BMPR1A, CASP8, CCL20, CCL21, COCH, CXCR2, FURIN, HSD3B1, ITPKB, MYBPC3, NUP98, PDGFB, PRF1, SMAD1, STAR, STAT6, TEAD4, ZNF423	ALDH3A1, CHRNA4, GP2, HMGN1, HRH2, IL18, MYCBP, RC3H1, ROCK2

↑ up-regulated; ↓ down-regulated

F **11-12 months Network 1 (most altered)**

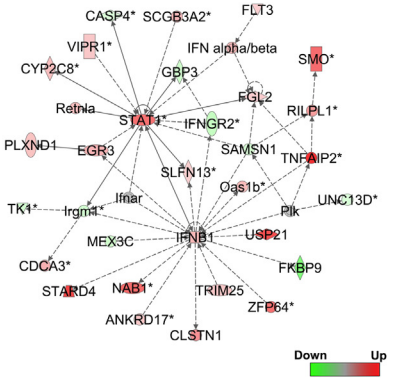

Fig. 2. Top five gene networks, and respective biological functions, specifically altered in the CP of J20 mice at different ages. The Ingenuity® Pathway Analysis setup computed the five most altered gene networks in the CP of J20 mice at 3 (A), 5–6 (C) and 11–12 (E) months, on the basis of the significantly up- (red) and down-regulated (green) genes, obtained after normalization to the expression levels in age-matched WT mice. An interaction scheme was assembled with the genes that composed the most altered network in the CP of J20 mice at 3 (B), 5–6 (D) and 11–12 (F) months.

overexpression of type I IFN genes in the dHPC of J20 mice at 3 months, when compared to age-matched WT mice, that was statistically significant for *Tlr9*, *Ifna1* and *Ifnb1* (Fig. 5A, D and E). Additionally, we observed a progressive increase in the expression of all type I IFN genes, with aging, in the dHPC of WT mice, which was statistically significant at 11–12 months, when compared to the expression levels of WT mice at 3 months (Fig. 5A–E). Regarding the expression of type II IFN genes in the dHPC (Fig. 5F and G), even though there was an increased expression of *Icam1* in 11–12 months-old WT mice (Fig. 5G), no changes were observed on the levels of *Ifng* expression at the different ages (Fig. 5F).

In an attempt to unravel the specific contribution of different brain cell populations to the overexpression of type I and II IFN genes, we measured the expression of *Tlr9*, *Ifna1* and *Ifng* in primary cultures of astrocytes and of neurons, at different time points upon stimulation with vehicle or 1 μM $A\beta_{1-42}$. However, no statistical significant differences were observed when comparing

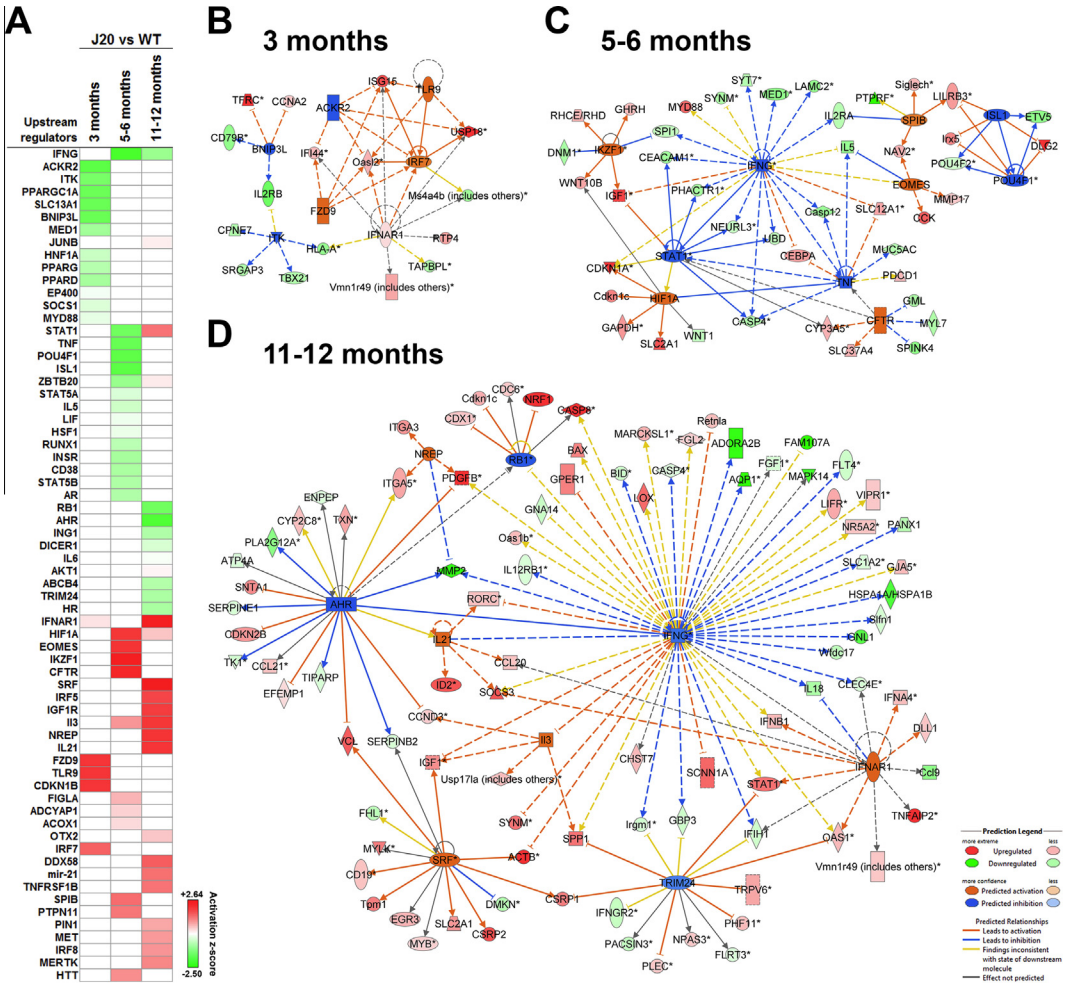

Fig. 3. Interactome of altered transcriptional regulators predicted an early activation of a type I IFN response and a later inactivation of a type II IFN response, in the CP of J20 mice. (A) The Ingenuity® Upstream Regulator Analysis computed an activation *z*-score for the transcriptional regulators that were predicted to modulate the gene expression alterations in the CP of J20 at different ages, after normalization to the expression levels in the CP of age-matched WT mice. A gene interactome was assembled at 3 (B), 5–6 (C) and 11–12 (D) months, using the five transcriptional regulators with highest activation *z*-score and the five transcriptional regulators with lowest activation *z*-score (Supplementary Table 3), as well as the significantly altered genes under their regulation, in each dataset. (B) The gene interactome at 3 months indicated an activation of TLR9, IRF7 and IFNAR1, characteristic of a type I IFN response. (C) At 5–6 months, the gene interactome underlined a down-regulation of IFN-γ, impacting on 18 downstream genes. (D) The down-regulation of IFN-γ was sustained at 11–12 months and its effect was even more pronounced, influencing the expression of 25 target genes.

vehicle- or $A\beta_{1-42}$-treated cells at 24 and 72 h (Supplementary Fig. 4).

3.6. Early activation of astrocytes and microglia was observed in the dHPC of J20 mice

To have a different readout of the inflammatory response in the dHPC of WT and J20 mice at different ages, we measured the expression of *Gfap* and *Iba1*, as well as the morphology of astrocytes and the number of microglia/macrophages from the DG of the dHPC, based on the staining for GFAP and IBA1, respectively (Fig. 5H–K). There was a significant overexpression of *Gfap* and *Iba1* in the dHPC of J20 mice, at 3 months, when compared to the expression levels in age-matched WT mice (Fig. 5H and J). The expression of *Gfap* was also significantly increased in the dHPC of WT mice at 11–12 months (Fig. 5H). Regarding the morphological characterization of astrocytes, overall, we observed that astrocytes from the dHPC of J20 mice presented a more ramified phenotype at 3 months, whereas, in the WT mice, these morphological alterations were observed at the age of 5–6 months (Fig. 5I). In that sense, except for the number of processes, a significant increase in the values of the analyzed astrocytic morphological parameters (length of individual processes, total surface and number of endings) was observed in astrocytes from the DG of J20 mice at 3 months, when compared to 3 months-old WT mice and to 5–6 months-old J20 mice (Fig. 5I). Noticeably, at 5–6 months, the astrocytes from the DG of WT mice presented more processes and were larger and more ramified than those of 5–6 months-old J20 mice and of 3 months- and 11–12 months-old mice of the same genotype (Fig. 5I). Concerning the quantification of microglia/-macrophages, there was a significant increase in the number of $IBA1^+$ cells per mm^2 in the DG of the dHPC of J20 mice at 11–12 months, when compared to all other groups (Fig. 5K).

3.7. Increased level of IFN-α in the CSF was correlated with a worst performance in the MWM

The level of IFN-α was measured in the CSF of WT and J20 mice, at different ages (Fig. 6A). Although not significant, we observed a tendency for an increased level of IFN-α in the CSF of J20 mice, when compared to 3 months-old WT mice, which was sustained over time (Fig. 6A). Interestingly, we observed a significant increase in the level of IFN-α in the CSF of WT mice at 5–6 and at 11–12 months, when compared to 3 months-old WT mice

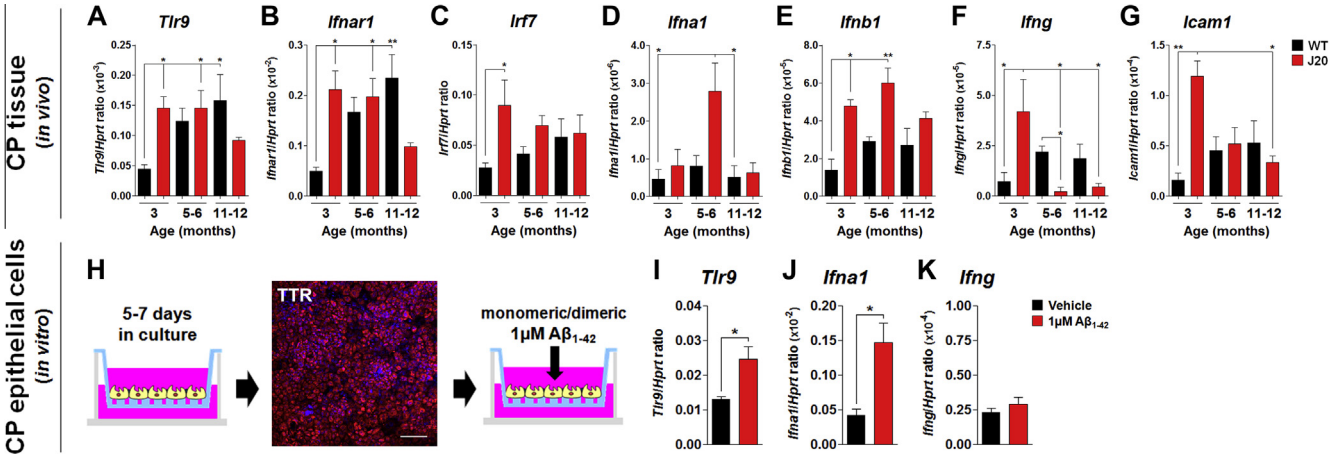

Fig. 4. CP epithelial cells contributed differently to the overexpression of type I and II IFN genes in response to increased levels of Aβ peptides. (A–G) The expression of type I and II IFN genes in the CP was measured by qRT-PCR. Except for *Ifna1*, all the genes were significantly overexpressed in the CP of J20 mice at 3 months when compared to the expression in age-matched WT. At 5–6 months, the overexpression of *Tlr9* (A), *Ifnar1* (B) and *Ifnb1* (E) was maintained in the CP of J20 mice, along with a significant overexpression of *Ifna1* (D). Also in the CP of J20 mice at 5–6 months, there was a significant down-regulation of *Ifng* (F), when compared to expression levels in J20 mice at 3 months and in WT mice at 5–6 months. (F, G) Both the expression of *Ifng* and *Icam1* were significantly decreased in the CP of J20 mice at 11–12 months, when compared to the expression levels at 3 months. (A, B) In the CP of WT mice, we observed a significant overexpression of *Tlr9* and *Ifnar1* at 11–12 months, when compared to the expression levels at 3 months. (H-K) Treatment of primary cultures of CP epithelial cells, which are composed by $\geqslant$ 95% of TTR$^+$ cells, with 1 μM Aβ_{1-42} for 60 h induced a significant overexpression of *Tlr9* (I) and *Ifna1* (J), but not of *Ifng* (K). Results regarding *in vivo* gene expression (A–G) are presented as mean ± SEM (N = 5/group); $^{*}p < 0.05$ and $^{**}p < 0.01$; Kruskal–Wallis with Dunns' multiple comparison test (two-tailed). Results regarding *in vitro* gene expression (I–K) are presented as mean ± SEM (N = 4/group); $^{*}p < 0.05$; two-tailed Mann Whitney test. Scale bar indicates 100 μm in (H).

(Fig. 6A), which was positively correlated with an increased time to find the hidden platform in the MWM (calculated as the average time of latency to platform in the five days of the test) (Fig. 6B). However, no significant correlations were observed between the levels of IFN-α and the latency to platform, when analyzing mice at each age separately (Supplementary Fig. 5).

In order to analyze the effects of age, genotype and IFN-α levels in the CSF as predictors of the spatial-reference memory performance, we designed two regression models, to take into consideration the main effects of the independent variables alone or all the possible interactions (Table 2). The genotype and the levels of IFN-α in the CSF, alone, were significantly associated with alterations in the performance in the MWM (model 1, Table 2). However, when the interactions between the independent variables were considered, the genotype significantly moderated the relation between age and latency (model 2, Table 2). Of relevance, when comparing the two models, the inclusion of the interaction effects only represented an increment of 4.65% in the explained variance of latency which was of 67.12% when no interactions were included in the analysis.

4. Discussion

A progressive dysfunction of the blood–CSF barrier, which is formed by the CP epithelial cells, is described in AD (Johanson et al., 2004; Marques et al., 2013; Serot et al., 2012). To better understand the specific alterations that occur at this barrier, we used the J20 mouse model of AD (Baron et al., 2014; Mucke et al., 2000) and investigated the changes in the CP transcriptome at the ages of 3, 5–6 and 11–12 months, in comparison with age-matched WT mice. We observed aging-induced alterations in the CP transcriptome involving gene networks that regulate central processes, such as the cellular circadian rhythm (Zhang and Kay, 2010), which are likely to affect the metabolic activity and cytoarchitecture of the blood–CSF barrier and to contribute to a defective turnover of the CSF (He et al., 2014; Serot et al., 2012).

Regarding the CP of J20 mice, there was a sustained overexpression of genes that participate in the type I IFN response and a clear decrease in the expression of *Ifng*, the major type II IFN gene. In a later age, but following the same direction, the CP of WT mice displayed an aging-associated increased expression of genes that encode for two receptors that are involved in the type I IFN response, *Tlr9* and *Ifnar1*, but no significant alterations in the expression of genes involved in the type II IFN response. Interestingly, the specific contribution of CP epithelial cells to the overexpression of type I IFN genes, but not of the type II IFN gene *Ifng*, shown to occur *in vitro* in response to Aβ, led us to suggest that the early overexpression of *Ifng* in the CP of J20 mice is due to immune-related cells that inhabit and circulate in the CP stromal compartment, a subject that warrants further investigation. Interestingly, the strong activation of the type I IFN response both in the CP and in the dHPC of J20 mice in early phases of the disease, before marked amyloid deposition, together with the decreased expression of *Ifng* in the CP at 5–6 and at 11–12 months, suggest a possible interplay between type I and II IFN responses and Aβ plaque formation. Moreover, although there is an apparent relationship between the up-regulation of type I IFN genes, the early overexpression of *Gfap* and *Iba1* and increased astrocytic branching in the dHPC, occurring first in J20 and later in WT mice, it is still unclear whether these observations are somehow connected. Of notice, together with a lower expression of type I IFN genes a decreased branching of astrocytes and increased number of microglia/macrophages was also found in the DG of the dHPC of J20 mice at 11–12 months. Intriguingly, also at 11–12 months, along with a decreased inflammatory gene expression in the dHPC, the behavioral impairment of J20 mice seems to become milder, when compared to 3 months-old mice of the same genotype. Once again, whether there is a causal relationship between these events in the brain of J20 mice and the deficits in memory is something that needs to be addressed in the future. In addition, an age-dependent increased level of IFN-α in the CSF, observed only in WT mice, is correlated with a poor performance in a spatial reference-memory task. On the other hand, the J20 mice presented no significant alterations in the level of IFN-α in the CSF, which is in agreement with their early and sustained memory impairment. In fact, it is still controversial whether an early induction of a type I IFN inflammatory response in the brain, followed by a reduced type II IFN response, is beneficial or detrimental for AD

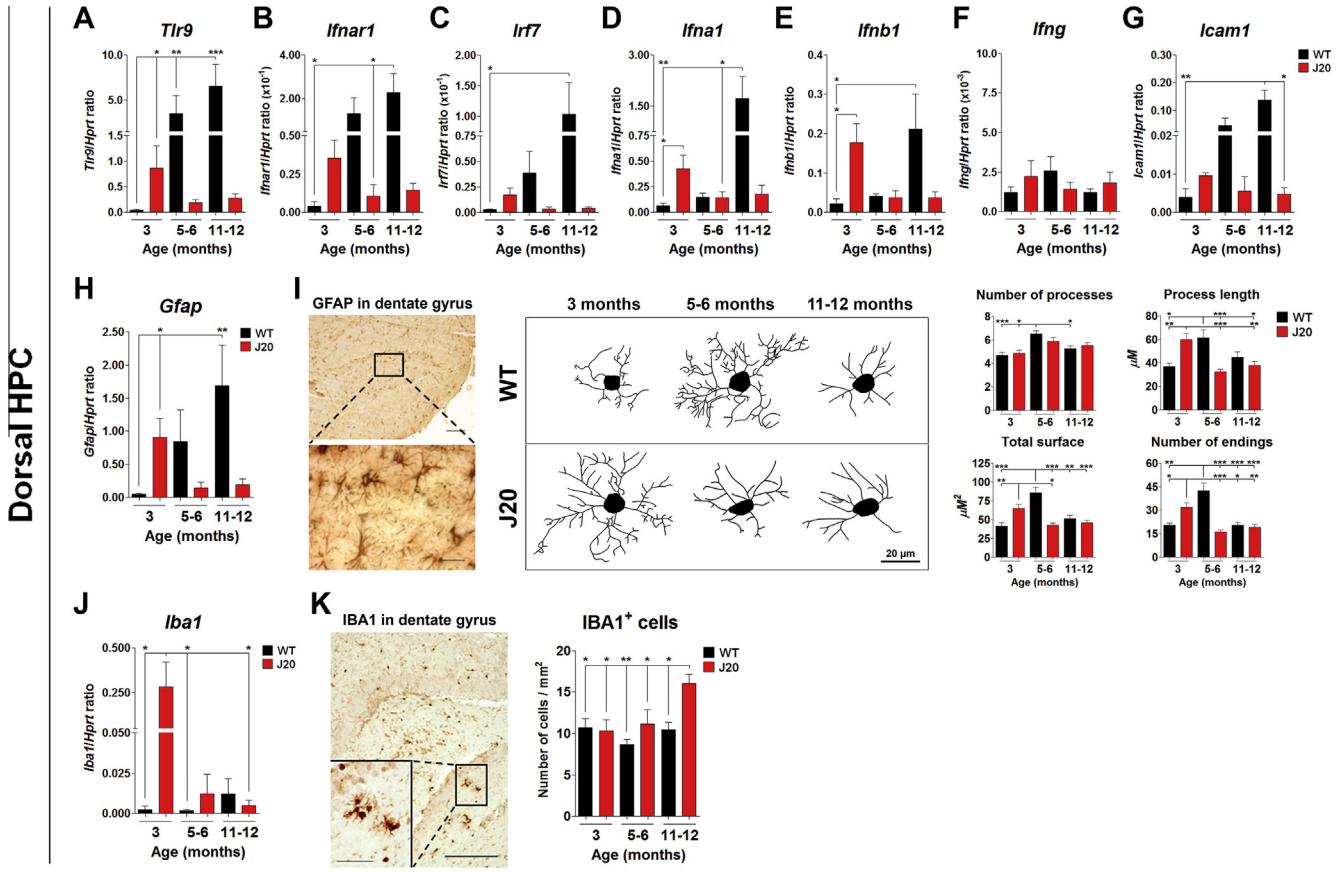

Fig. 5. Aging altered the pattern of type I and II IFN gene expression, the morphology of astrocytes and the number of microglia/macrophages in the dHPC of WT and J20 mice. (A–G) The expression of type I and II IFN genes in the dHPC was measured by qRT-PCR. A significant overexpression of the type I IFN genes *Tlr9* (A), *Ifna1* (D) and *Ifnb1* (E) was observed in the dHPC of J20 mice at 3 months. On the other hand, at 11–12 months, except for *Ifng* (F), there was a statistically significant overexpression of all genes in the dHPC of WT mice. (H, I) To correlate the type I IFN gene expression with a different readout of the inflammatory status in the dHPC, the expression of *Gfap* and the morphology of astrocytes was analyzed in the DG. (H) There was a significant overexpression of *Gfap* in the dHPC of J20 and WT mice, at 3 and 11–12 months, respectively. (I) A significant increase in the size and number of endings of the astrocytic processes and, consequently, in the total surface of astrocytes, was observed in the DG of the dHPC of J20 mice at 3 months. In contrast, at 5–6 months and 11–12 months, the astrocytes of the DG of J20 mice presented less ramified processes and occupied a smaller surface. Noticeably, the astrocytes from the DG of WT mice presented a significant increase in all the analyzed morphological parameters at 5–6 months, but became significantly smaller and less ramified at 11–12 months. (J) There was a significant overexpression of *Iba1* in the dHPC of J20 mice at 3 months. (K) The number of IBA1$^+$ cells per mm^2 in the DG of 11–12 months-old J20 mice was significantly higher when compared to all other groups. Results regarding gene expression are presented as mean ± SEM (N = 5/group); $^{*}p < 0.05$, $^{**}p < 0.01$ and $^{***}p < 0.001$; Kruskal–Wallis with Dunns' multiple comparison test (two-tailed). Results regarding astrocytic morphology in (I) are presented as mean ± SEM (N = 30 astrocytes/group) and microglia/macrophages in (K) are presented as mean ± SEM (N = 4/group at 3 and 5–6 months, and N = 5/group at 11–12 months); $^{*}p < 0.05$, $^{**}p < 0.01$ and $^{***}p < 0.001$; Kruskal–Wallis with Dunns' multiple comparison test (two-tailed). Scale bars indicate 100 µm (lower magnification) and 20 µm (higher magnification) in (I) and 200 µm (lower magnification) and 50 µm (higher magnification) in (K).

pathogenesis (Baruch et al., 2014; Scholtzova et al., 2009, 2014; Taylor et al., 2014). Regarding the type II IFN response in AD, it has been previously shown that overexpression of IFN-γ boosts the amyloidogenic processing of APP both *in vitro* and *in vivo* (Blasko et al., 1999; Mastrangelo et al., 2009). In accordance, it was recently suggested that a higher frequency of IFN-γ-producing T-cells in the brain of AD transgenic mice is associated with increased glial activation and amyloid plaque formation, as well as with worst cognitive function (Browne et al., 2013). However, there is also evidence of a beneficial impact of increased levels of IFN-γ-producing T-cells in AD transgenic mice at 9 months of age, namely by increased microglial activation, increased Aβ phagocytosis and decreased plaque burden in the DG of the HPC (Monsonego et al., 2006). These divergent observations may be due to the specific effects of IFN-γ overproduction at different stages of brain pathology in AD, which prompts for a deeper characterization of the role of the type II IFN mediators in the AD brain at different ages. On the other hand, concerning the type I IFN response, a recent study showed that at the level of the CP of 22 months-old mice, increased levels of IFN-β signaling promote increased glial activation and impact on cognitive behavior (Baruch et al., 2014). Moreover, it was suggested that an aging-related central nervous system (CNS)-derived stimulus could be in the genesis of a shift from a type II IFN into a type I IFN response at the CP, and that this would compromise the immune-surveillance of the brain by decreasing the levels of IFN-γ (Baruch et al., 2014; Kunis et al., 2013). Interestingly, even in the absence of a viral infection, increased levels of type I IFN cytokines in the brain, particularly IFN-α, lead to massive encephalopathy, with marked meningoencephalitis, calcium mineralization, gliosis, and neurodegeneration (Akwa et al., 1998). In the context of AD, others have shown that the genes encoding for IFN-α and IFN-β are overexpressed in cultured neurons, upon stimulation with Aβ, and in cortical cells extracted from the brains of AD patients, in a mechanism dependent on IRF7 and IFNAR1, which is associated with decreased neuronal viability (Taylor et al., 2014). Conversely, stimulation of the innate response with the TLR9 agonists cytosine-guanosine-containing DNA oligodeoxynucleotides (CpG DNA oligos), in two different mouse models of AD, ameliorated both the pathologic hallmarks and the

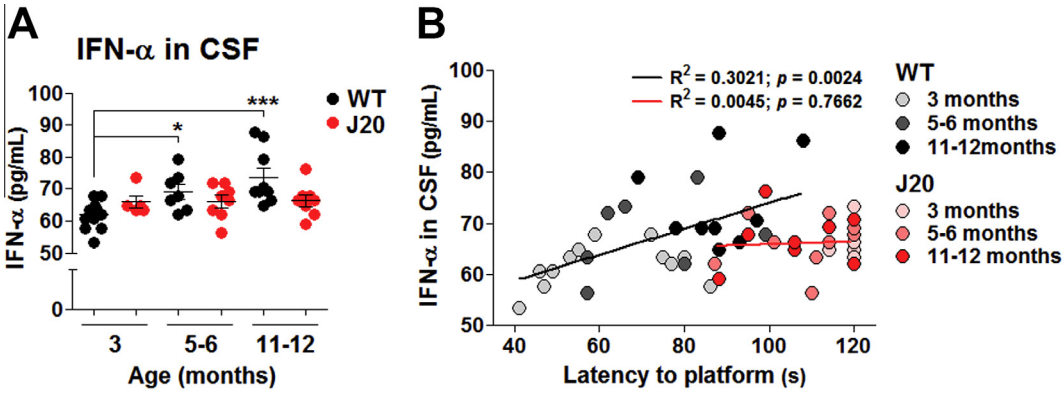

Fig. 6. Age-dependent increased level of IFN-α in the CSF of WT mice was significantly correlated with a worst memory function. (A) The level of IFN-α was significantly increased in the CSF of WT mice at 5–6 and 11–12 months, when compared to 3 months-old mice of the same genotype. Of notice, although not statistically significant, a tendency for an increased level of IFN-α was observed in the CSF of 3 months-old J20 mice, when compared to the levels measured in 3 months-old WT mice, which was sustained over time. (B) A positive correlation between the level of IFN-α in the CSF of WT mice and the average time of latency to platform in the five days of the MWM (gray to black dots) was observed. No correlation was found between the levels of IFN-α in the CSF and the latency to platform in J20 mice (pink to red dots). Results regarding the measurement of IFN-α are presented as mean ± SEM [3 months: N (WT) = 12 and N (J20) = 5; 5–6 months: N (WT) = 7 and N (J20) = 8; 11–12 months: N (WT) = 9 and N (J20) = 8]; $^{*}p < 0.05$ and $^{***}p < 0.001$; Kruskal–Wallis with Dunns' multiple comparison test (two-tailed). The Pearson's correlation test was used to perform the analysis in (B) and to calculate the associated R^2 and p-value (two-tailed). Correlation was considered significant for $p < 0.05$; N (WT) = 28 and N (J20) = 22.

cognitive deficits presented by these mice, without any obvious inflammatory side-effects (Scholtzova et al., 2009, 2014). Also, increased production of IFN-β by astrocytes, upon specific TLR3 stimulation, was shown to affect the spontaneous activity of neurons from the CA1 region of the HPC. This effect of IFN-β on neuronal excitability was shown to be mediated by IFNAR1, due to the lack of changes in the HPC of *Ifnra1*-null mice (Costello and Lynch, 2013). Additionally, 9 months-old transgenic APP/PS1 mice present higher levels of IFN-α in the brain, when compared to age-matched WT mice (Taylor et al., 2014). Interestingly, our results also suggest that, along with a possible impact on behavior, an activation of a type I IFN response in the dHPC, in younger J20 mice and in 11–12 months-old WT mice may be linked with changes in the astrocytes' morphology. It is widely accepted that increased levels of inflammatory molecules, whether in the circulation or in specific regions of the CNS, can affect the morphology and function of brain cells, especially of glial cells (Baron et al., 2014; Ghosh et al., 2013). Astrocytes in particular seem to play a central role in the inflammatory response and are good indicators of the level of brain inflammation (Medeiros and LaFerla, 2013; Wyss-Coray, 2006). Concurrently, the activation of astrocytes and microglia was shown to occur before Aβ plaque formation in the HPC of J20 mice (Baron et al., 2014; Beauquis et al., 2014; Wright et al., 2013) and that an increased microglial activation and clustering, observed at 4 weeks of age in the HPC of these mice, precedes neuronal atrophy, decreased neurogenesis and a decrease in the volume of the HPC (Fu et al., 2014). However, it is necessary to further investigate whether the early induction of type I IFN genes in the dHPC of J20 mice is directly promoting changes in glial activation and Aβ pathology. Moreover, it will be important to explore the impact of increased level of type I IFN cytokines, such as IFN-α, on the premature memory deficits observed in this AD mouse model and on the memory and cognitive impairments in older WT mice.

Overall, this study reveals that structures such as the CP and the dHPC may be key elements in the inflammatory signaling in the CNS, by modulating the levels of IFNs, with a possible impact on memory and cognition.

Competing interests

The authors have no conflicting financial interests to declare.

Database linking

According to the Minimum Information About a Microarray Experiment (MIAME), the microarray raw data has been deposited in the GEO database, with the accession number GEO: GSE66598.

Acknowledgments

The authors would like to acknowledge Pedro Moreira, Madalena Esteves and Dr. Patrício Costa (all from the ICVS/3B's – PT Government Associate Laboratory) for comments and scientific input regarding the statistical analysis of this study. Sandro Dá Mesquita and Ana C. Ferreira are recipients of PhD fellowships by the Fundação para a Ciência e Tecnologia (FCT, Portugal)/FEDER and Programa Operacional Potencial Humano (POPH/FSE), references SFRH/BD/69706/2010 and SFRH/BD/51989/2012, respectively. Fernanda Marques is an assistant researcher and recipient of a FCT Investigator Grant with the reference IF/00231/2013. This work was supported by FCT and COMPETE through the project EXPL/NEU-OSD/2196/2013 and the Bial Foundation through the Grant 217/12.

Appendix A. Supplementary data

Supplementary data associated with this article can be found, in the online version, at http://dx.doi.org/10.1016/j.bbi.2015.06.008.

References

Akwa, Y., Hassett, D.E., Eloranta, M.L., Sandberg, K., Masliah, E., Powell, H., Whitton, J.L., Bloom, F.E., Campbell, I.L., 1998. Transgenic expression of IFN-alpha in the central nervous system of mice protects against lethal neurotropic viral infection but induces inflammation and neurodegeneration. J. Immunol. 161, 5016–5026.

Ballard, C., Gauthier, S., Corbett, A., Brayne, C., Aarsland, D., Jones, E., 2011. Alzheimer's disease. Lancet 377, 1019–1031.

Baron, R., Babcock, A.A., Nemirovsky, A., Finsen, B., Monsonego, A., 2014. Accelerated microglial pathology is associated with Abeta plaques in mouse models of Alzheimer's disease. Aging Cell 13, 584–595.

Baruch, K., Schwartz, M., 2013. CNS-specific T cells shape brain function via the choroid plexus. Brain Behav. Immun. 34, 11–16.

Baruch, K., Ron-Harel, N., Gal, H., Deczkowska, A., Shifrut, E., Ndifon, W., Mirlas-Neisberg, N., Cardon, M., Vaknin, I., Cahalon, L., Berkutzki, T., Mattson, M.P., Gomez-Pinilla, F., Friedman, N., Schwartz, M., 2013. CNS-specific immunity at the choroid plexus shifts toward destructive Th2 inflammation in brain aging. Proc. Natl. Acad. Sci. USA 110, 2264–2269.

Baruch, K., Deczkowska, A., David, E., Castellano, J.M., Miller, O., Kertser, A., Berkutzki, T., Barnett-Itzhaki, Z., Bezalel, D., Wyss-Coray, T., Amit, I., Schwartz, M., 2014. Aging-induced type I interferon response at the choroid plexus negatively affects brain function. Science 346, 89–93.

Beauquis, J., Vinuesa, A., Pomilio, C., Pavia, P., Galvan, V., Saravia, F., 2014. Neuronal and glial alterations, increased anxiety, and cognitive impairment before hippocampal amyloid deposition in PDAPP mice, model of Alzheimer's disease. Hippocampus 24, 257–269.

Blasko, I., Marx, F., Steiner, E., Hartmann, T., Grubeck-Loebenstein, B., 1999. TNFalpha plus IFNgamma induce the production of Alzheimer beta-amyloid peptides and decrease the secretion of APPs. FASEB J. 13, 63–68.

Browne, T.C., McQuillan, K., McManus, R.M., O'Reilly, J.A., Mills, K.H., Lynch, M.A., 2013. IFN-gamma Production by amyloid beta-specific Th1 cells promotes microglial activation and increases plaque burden in a mouse model of Alzheimer's disease. J. Immunol. 190, 2241–2251.

Carro, E., Trejo, J.L., Gomez-Isla, T., LeRoith, D., Torres-Aleman, I., 2002. Serum insulin-like growth factor I regulates brain amyloid-beta levels. Nat. Med. 8, 1390–1397.

Carro, E., Spuch, C., Trejo, J.L., Antequera, D., Torres-Aleman, I., 2005. Choroid plexus megalin is involved in neuroprotection by serum insulin-like growth factor I. J. Neurosci. 25, 10884–10893.

Coppola, G., 2011. Designing, performing, and interpreting a microarray-based gene expression study. Methods Mol. Biol. 793, 417–439.

Coppola, G., Karydas, A., Rademakers, R., Wang, Q., Baker, M., Hutton, M., Miller, B.L., Geschwind, D.H., 2008. Gene expression study on peripheral blood identifies progranulin mutations. Ann. Neurol. 64, 92–96.

Costello, D.A., Lynch, M.A., 2013. Toll-like receptor 3 activation modulates hippocampal network excitability, via glial production of interferon-beta. Hippocampus 23, 696–707.

Fu, Y., Rusznak, Z., Kwok, J.B., Kim, W.S., Paxinos, G., 2014. Age-dependent alterations of the hippocampal cell composition and proliferative potential in the hAbetaPPSwInd-J20 mouse. J. Alzheimers Dis. 41, 1177–1192.

Ghosh, S., Wu, M.D., Shaftel, S.S., Kyrkanides, S., LaFerla, F.M., Olschowka, J.A., O'Banion, M.K., 2013. Sustained interleukin-1beta overexpression exacerbates tau pathology despite reduced amyloid burden in an Alzheimer's mouse model. J. Neurosci. 33, 5053–5064.

Gotz, J., Chen, F., van Dorpe, J., Nitsch, R.M., 2001. Formation of neurofibrillary tangles in P301l tau transgenic mice induced by Abeta 42 fibrils. Science 293, 1491–1495.

Hardy, J., Selkoe, D.J., 2002. The amyloid hypothesis of Alzheimer's disease: progress and problems on the road to therapeutics. Science 297, 353–356.

He, J., Hsuchou, H., He, Y., Kastin, A.J., Wang, Y., Pan, W., 2014. Sleep restriction impairs blood–brain barrier function. J. Neurosci. 34, 14697–14706.

Johanson, C., McMillan, P., Tavares, R., Spangenberger, A., Duncan, J., Silverberg, G., Stopa, E., 2004. Homeostatic capabilities of the choroid plexus epithelium in Alzheimer's disease. Cerebrospinal Fluid Res. 1, 3.

Kunis, G., Baruch, K., Rosenzweig, N., Kertser, A., Miller, O., Berkutzki, T., Schwartz, M., 2013. IFN-gamma-dependent activation of the brain's choroid plexus for CNS immune surveillance and repair. Brain 136, 3427–3440.

Lewis, J., Dickson, D.W., Lin, W.L., Chisholm, L., Corral, A., Jones, G., Yen, S.H., Sahara, N., Skipper, L., Yager, D., Eckman, C., Hardy, J., Hutton, M., McGowan, E., 2001. Enhanced neurofibrillary degeneration in transgenic mice expressing mutant tau and APP. Science 293, 1487–1491.

Lucin, K.M., Wyss-Coray, T., 2009. Immune activation in brain aging and neurodegeneration: too much or too little? Neuron 64, 110–122.

Marques, F., Sousa, J.C., Coppola, G., Falcao, A.M., Rodrigues, A.J., Geschwind, D.H., Sousa, N., Correia-Neves, M., Palha, J.A., 2009. Kinetic profile of the transcriptome changes induced in the choroid plexus by peripheral inflammation. J. Cereb. Blood Flow Metab. 29, 921–932.

Marques, F., Sousa, J.C., Sousa, N., Palha, J.A., 2013. Blood–brain-barriers in aging and in Alzheimer's disease. Mol. Neurodegener. 8, 38.

Mastrangelo, M.A., Sudol, K.L., Narrow, W.C., Bowers, W.J., 2009. Interferon-{gamma} differentially affects Alzheimer's disease pathologies and induces neurogenesis in triple transgenic-AD mice. Am. J. Pathol. 175, 2076–2088.

Mazen, A.M.M., Hemmasi, M., Lewis, M.F., 1985. In search of power: a statistical power analysis of contemporary research in strategic management. Acad. Manage. Proc. 1985, 30–34.

Medeiros, R., LaFerla, F.M., 2013. Astrocytes: conductors of the Alzheimer disease neuroinflammatory symphony. Exp. Neurol. 239, 133–138.

Mesquita, S.D., Ferreira, A.C., Falcao, A.M., Sousa, J.C., Oliveira, T.G., Correia-Neves, M., Sousa, N., Marques, F., Palha, J.A., 2014. Lipocalin 2 modulates the cellular response to amyloid beta. Cell Death Differ. 21, 1588–1599.

Monsonego, A., Imitola, J., Petrovic, S., Zota, V., Nemirovsky, A., Baron, R., Fisher, Y., Owens, T., Weiner, H.L., 2006. Abeta-induced meningoencephalitis is IFN-gamma-dependent and is associated with T cell-dependent clearance of Abeta in a mouse model of Alzheimer's disease. Proc. Natl. Acad. Sci. USA 103, 5048–5053.

Mucke, L., Masliah, E., Yu, G.Q., Mallory, M., Rockenstein, E.M., Tatsuno, G., Hu, K., Kholodenko, D., Johnson-Wood, K., McConlogue, L., 2000. High-level neuronal expression of abeta 1–42 in wild-type human amyloid protein precursor transgenic mice: synaptotoxicity without plaque formation. J. Neurosci. 20, 4050–4058.

Palop, J.J., Mucke, L., 2010. Amyloid-beta-induced neuronal dysfunction in Alzheimer's disease: from synapses toward neural networks. Nat. Neurosci. 13, 812–818.

Palop, J.J., Chin, J., Roberson, E.D., Wang, J., Thwin, M.T., Bien-Ly, N., Yoo, J., Ho, K.O., Yu, G.Q., Kreitzer, A., Finkbeiner, S., Noebels, J.L., Mucke, L., 2007. Aberrant excitatory neuronal activity and compensatory remodeling of inhibitory hippocampal circuits in mouse models of Alzheimer's disease. Neuron 55, 697–711.

Querfurth, H.W., LaFerla, F.M., 2010. Alzheimer's disease. N. Engl. J. Med. 362, 329–344.

Roberson, E.D., Mucke, L., 2006. 100 years and counting: prospects for defeating Alzheimer's disease. Science 314, 781–784.

Scheuner, D., Eckman, C., Jensen, M., Song, X., Citron, M., Suzuki, N., Bird, T.D., Hardy, J., Hutton, M., Kukull, W., Larson, E., Levy-Lahad, E., Viitanen, M., Peskind, E., Poorkaj, P., Schellenberg, G., Tanzi, R., Wasco, W., Lannfelt, L., Selkoe, D., Younkin, S., 1996. Secreted amyloid beta-protein similar to that in the senile plaques of Alzheimer's disease is increased in vivo by the presenilin 1 and 2 and APP mutations linked to familial Alzheimer's disease. Nat. Med. 2, 864–870.

Scholtzova, H., Kascsak, R.J., Bates, K.A., Boutajangout, A., Kerr, D.J., Meeker, H.C., Mehta, P.D., Spinner, D.S., Wisniewski, T., 2009. Induction of toll-like receptor 9 signaling as a method for ameliorating Alzheimer's disease-related pathology. J. Neurosci. 29, 1846–1854.

Scholtzova, H., Chianchiano, P., Pan, J., Sun, Y., Goni, F., Mehta, P.D., Wisniewski, T., 2014. Amyloid beta and Tau Alzheimer' disease related pathology is reduced by Toll-like receptor 9 stimulation. Acta Neuropathol. Commun. 2, 101.

Serot, J.M., Zmudka, J., Jouanny, P., 2012. A possible role for CSF turnover and choroid plexus in the pathogenesis of late onset Alzheimer's disease. J. Alzheimers Dis. 30, 17–26.

Sousa, J.C., Cardoso, I., Marques, F., Saraiva, M.J., Palha, J.A., 2007. Transthyretin and Alzheimer's disease: where in the brain? Neurobiol. Aging 28, 713–718.

Taylor, J.M., Minter, M.R., Newman, A.G., Zhang, M., Adlard, P.A., Crack, P.J., 2014. Type-1 interferon signaling mediates neuro-inflammatory events in models of Alzheimer's disease. Neurobiol. Aging 35, 1012–1023.

Villeda, S.A., Luo, J., Mosher, K.I., Zou, B., Britschgi, M., Bieri, G., Stan, T.M., Fainberg, N., Ding, Z., Eggel, A., Lucin, K.M., Czirr, E., Park, J.S., Couillard-Despres, S., Aigner, L., Li, G., Peskind, E.R., Kaye, J.A., Quinn, J.F., Galasko, D.R., Xie, X.S., Rando, T.A., Wyss-Coray, T., 2011. The ageing systemic milieu negatively regulates neurogenesis and cognitive function. Nature 477, 90–94.

Wright, A.L., Zinn, R., Hohensinn, B., Konen, L.M., Beynon, S.B., Tan, R.P., Clark, I.A., Abdipranoto, A., Vissel, B., 2013. Neuroinflammation and neuronal loss precede Abeta plaque deposition in the hAPP-J20 mouse model of Alzheimer's disease. PLoS ONE 8, e59586.

Wyss-Coray, T., 2006. Inflammation in Alzheimer disease: driving force, bystander or beneficial response? Nat. Med. 12, 1005–1015.

Zhang, E.E., Kay, S.A., 2010. Clocks not winding down: unravelling circadian networks. Nat. Rev. Mol. Cell Biol. 11, 764–776.

Zlokovic, B.V., 2008. The blood–brain barrier in health and chronic neurodegenerative disorders. Neuron 57, 178–201.